*Proc. of the European Safety and Reliability Conference (ESREL 2026)*
*Edited by* José C. Matos, Paulo B. Lourenço, Michael Beer, Daniel Oliveira, Edoardo Patelli, Hélder S. Sousa, Rui A. Silva and Monica Santamaria

doi: 10.3850/ESREL2026061419_esrel26-p27858-cd

# Climate Change Impact on Railway Track Buckling: A Probabilistic Risk Assessment for Taiwan

I-Kai Lu

*Master Student, Department of Civil Engineering, National Yang Ming Chiao Tung University, Taiwan.*
*E-mail: jimmy891213sam@gmail.com*

Chi-Ying Lin

*Assistant Professor, Department of Civil Engineering, National Yang Ming Chiao Tung University, Taiwan.*
*E-mail: chiyinglin@nycu.edu.tw*

This study examines the risk of heat-induced rail buckling on the mainline network of Taiwan Railways Corporation (TRC) under historical and future climate conditions. As extreme heat events become more frequent under climate change, railway infrastructure faces increasing exposure to thermally induced instability. TRC has recorded the highest number of natural hazard-related incidents among Taiwan's railway operators, including recurrent buckling events and a major derailment in 2016. This study aims to estimate the temporal variation and spatial distribution of rail buckling risk. A physics-based probabilistic framework was developed for ballasted continuous welded rail by integrating analytical buckling models, Monte Carlo simulation, railway geometry, rail–air temperature regression, and climate projection data. Three analytical models—Meier, Sato, and Bae—were adopted for comparison. Future climate inputs for 2025–2100 were derived from the TaiESM model under the IPCC AR6 SSP1-2.6, SSP2-4.5, SSP3-7.0, and SSP5-8.5 scenarios, and the network was discretized into 20 m analysis units. Historical records indicate 75 buckling incidents during 1990–2023, more than 90% of which occurred between April and September. Back-casting results show that the Bae model produced the closest agreement with Bayesian validation based on observed event frequencies. Future projections suggest limited change under SSP1-2.6 but increasing summer buckling risk under higher-emissions scenarios. Historical incidents were concentrated in northern and central Taiwan, and projected risk maps show clear spatiotemporal variation across years and scenarios. Sensitivity analysis indicates that curve radius and lateral ballast resistance are key factors affecting buckling probability.

*Keywords*: Climate change, Rail buckling, Risk of railway network, High temperature, TRC, Ballast resistance force, Monte Carlo simulation

## 1. Introduction

### 1.1. *Impact of climate change on railway systems*

Climate change intensifies extreme weather events, posing significant threats to transportation infrastructure. The Taiwan Railway Corporation (TRC), a critical intercity network, has demonstrated vulnerability to these shifts, notably through the 2016 derailment caused by heat-induced rail buckling. Consequently, the Institute of Transportation (IOT) has prioritized the development of quantitative risk assessments and adaptation strategies for the island's rail systems.

### 1.2. *Research objectives*

The TRC is highly vulnerable to climate impacts and has recorded the greatest number of natural hazard-related incidents among Taiwan's rail operators. This study investigates heat-induced rail buckling on the TRC mainline network, focusing on temporal risk estimation and spatial hotspot identification.

Historical records document 75 buckling incidents during 1990–2023, including a major derailment in 2016 associated with rail temperatures of 63 °C. To assess future risk under climate change, this study integrates modified rail-buckling models with Monte Carlo simulation to project risk for 2025–2100 and identify high-risk segments, with additional validation using a Bayesian model based on historical events. The results support maintenance planning, operational adaptation, and long-term investment decisions.

## 2. Literature Review

### 2.1. *Definition and Mechanisms of Rail Buckling*

Continuous Welded Rail (CWR) improves ride quality by eliminating joints, but the resulting restraint of thermal expansion causes axial compressive stress to accumulate. Buckling occurs when this thermal force exceeds the track's lateral resistance, mainly provided by the ballast, sleepers, and fasteners, with ballast lateral resistance identified as the dominant factor. Although bridge-track interaction may affect stability, its influence on ballasted track is considered negligible relative to slab track (Chu, 2002; Luo et al., 2010). Accordingly, this study focuses on ballasted track, incorporating wheel-track dynamics but excluding bridge interaction.

### 2.2. *Quantitative Risk Assessment*

Risk assessment methods generally categorize into statistical analysis or physics-based modeling. Statistical approaches correlate historical failures with climate data (Dobney et al., 2009; Chinowsky et al., 2019), consistently predicting increased failure frequencies under future warming. Conversely, physics-based models combine mechanical theories with probabilistic simulations to estimate buckling probability. This approach defines parameters (e.g., lateral resistance, SFT) as distributions and uses Monte Carlo simulations to compare the thermal axial force ( $P_T$ ) against resistance strength. $P_T$ is calculated as Eq. (1):

$$P_T = EA\alpha(T_{rail} - T_{SFT}) \qquad (1)$$

Where $E$ is Young's modulus, $A$ is the cross-sectional area, and $\alpha$ is the thermal expansion coefficient. Following frameworks like Villalba Sanchis et al. (2020) and Nguyen et al. (2012), this study adopts a localized physics-based Monte Carlo simulation.

## 3. Data Acquisition and Processing

This study integrates analytical buckling models, standardized track and material parameters, rail–air temperature regression, railway geometry, and climate projection data to assess heat-induced rail buckling risk.

### 3.1. *Critical Buckling Formula*

Rail buckling prediction methods can be grouped into analytical, semi-analytical or energy-based, numerical, statistical or empirical, machine-learning, and hybrid approaches. This study adopts analytical models because of their interpretability and computational efficiency, with emphasis on critical buckling axial force and allowable temperature rise. Since most existing formulations were developed for ballasted track, slab track is excluded due to its much higher lateral and longitudinal restraint. Among the available analytical formulations, the Meier(Chiang 2017), Sato (Huang 2022), and Bae(Bae et al., 2014) models were selected to estimate buckling risk and compare model performance. Due to space limitations, only the formulation of the Sato model is provided in Appendix A. Other formulations, such as those of Bartlett, Kerr, and Schramm, were not included because they remain under testing and validation.

### 3.2. *Track and Material Parameters*

Rail properties for JIS 50N rail were adopted from Huang (2009), including cross-sectional area $A = 64.2\ \mathrm{cm}^2$, vertical-axis moment of inertia $J = 334\ \mathrm{cm}^4$, thermal expansion coefficient $\alpha = 1.14 \times 10^{-5}\ 1/°C$, and Young's modulus $E = 2.1 \times 10^6\ \mathrm{kgf/cm}^2$.

Several key uncertain parameters were modeled probabilistically. The rail laying temperature $T_{SFT}$ was represented by a normal distribution based on the common Taiwan Railways reference range of 35–40 °C. Lateral ballast resistance $g$ was characterized using maintenance specifications for 1067 mm gauge railways and 113 field measurements reported by Chen (2019). In Sato's model, the track panel rigidity ratio $N_j$ was conservatively set to 1.0. Track direction alignment irregularity $f_r$ was modeled as a normal distribution with mean 0 and standard deviation 6 mm, with half-wave length set to 5 m. Vertical ballast stiffness $VBS$ followed the normal distribution proposed by Bae et al. (2014). Train speed $V$ was assigned according to curve-radius-based operating limits, and the maximum allowable speed was adopted for conservatism.

### 3.3. *Rail–Air Temperature Relationship*

Although Han's rail-temperature model was initially considered, it requires hourly solar radiation and related variables that were not fully processed during the study period. Therefore, this study adopted a direct regression between observed rail temperature and air temperature. Future work will incorporate solar radiation to improve prediction accuracy.

### 3.4. *Railway Route and Climate Data*

Track geometry data from the Taiwan Land Surveying and Mapping Center were processed in QGIS to extract ballasted track segments, excluding tunnels and slab track. Historical and projected climate data were obtained from TCCIP (Taiwan Climate Change Projection Information and Adaptation Knowledge Platform). Future projections were based on the TaiESM model under IPCC AR6 scenarios SSP1-2.6, SSP2-4.5, SSP3-7.0, and SSP5-8.5, using statistically downscaled data for extreme heat assessment.

### 3.5. *Historical Buckling Events*

TRC records from 1990 to 2023 indicate that more than 90% of buckling events occurred during April–September, mainly between 10:00 and 15:00. Spatially, incidents were concentrated in northern and central Taiwan rather than in the hotter south, suggesting that ballast maintenance quality and insufficient lateral resistance are key contributors to risk.

Table 1. Regression results for first- to fourth-order polynomial models

| Polynomial Order | Training $R^2$ | Testing $R^2$ | MAE | RSE | Regression Equation |
|---|---|---|---|---|---|
| **1st Order** | 0.714 | 0.701 | 3.021 | 4.000 | $T_{rail} = -13.274 + 1.701\,T_{air}$ |
| **2nd Order** | 0.743 | 0.736 | 2.935 | 3.758 | $T_{rail} = -61.101 + 4.842\,T_{air} - 0.051\,{T_{air}}^2$ |
| **3rd Order** | 0.750 | 0.747 | 2.899 | 3.683 | $T_{rail} = 124.698 - 13.314\,T_{air} + 0.533\,{T_{air}}^2 - 0.006\,{T_{air}}^3$ |
| **4th Order** | 0.750 | 0.748 | 2.908 | 3.678 | $T_{rail} = 342.568 - 41.085\,T_{air} + 1.841\,{T_{air}}^2 - 0.033\,{T_{air}}^3 + 0.00021\,{T_{air}}^4$ |

## 4. Methodology

### 4.1. *Spatial Discretization and Matching*

The track network was discretized into 20 m analysis units to balance spatial resolution and computational efficiency. Curve radius was estimated from the circumscribed circle of three consecutive nodes resampled at 10 m intervals. Temperature inputs were matched to each unit using a kD-Tree nearest-neighbor algorithm, and monthly statistics of daily maximum temperature were integrated into the units database.

### 4.2. *Statistical Modelling of Lateral Resistance*

Based on 113 field measurements (Chen, 2019), Construction Branches were grouped into three clusters. Probability distributions were fitted using maximum likelihood estimation and evaluated with K-S tests and AIC/BIC. A reduction factor of 0.4 was applied to represent maintenance disturbance (UIC Code 720R, Hu et al., 2018).

### 4.3. *Rail Temperature Prediction*

A rail-temperature regression model was developed using historical data from seven Taiwan Railways monitoring stations, excluding Toucheng because of anomalous records. Only observations from 09:00–16:00 with air temperature above 22 °C were used, and incomplete records were removed. Monthly and station-based weighting was applied to reduce temporal and spatial imbalance.

Model performance was evaluated using $R^2$ and MAE (Table 1). Because higher-order polynomials provided only marginal improvement, a first-order regression was adopted for simplicity and more stable extrapolation under extreme temperatures. Predictive uncertainty was represented by a random error term, $k \sim N(0, RSE)$, where $RSE$ is the unbiased residual standard deviation estimated from the training data.

### 4.4. *Numerical Simulation Process*

A Monte Carlo simulation with $N = 1000$ was performed for each analysis unit. Buckling probability $(P_b)$was defined as the ratio of failure instances $(n)$to total trials (Eq. (3)), where failure occurred when the total axial force $(P_2)$exceeded the dynamic buckling resistance strength $(P_1)$(Eq. (2)).

$$P_1 \leq P_2 \qquad (2)$$

$$P_b = \frac{n}{N} \qquad (3)$$

$P_1$ denotes the dynamic buckling resistance strength, taken as 70% of the static strength $(P_{cr})$ to account for the uplift effect (Kish & Samavedam, 1991). $P_2$ denotes the total axial force, including thermal and braking forces. The braking force was estimated as 19.088 tons per rail based on the deceleration of a TRC EMU3000 trainset, whereas gradient-induced forces were neglected because they were small relative to braking loads.

## 5. Result

### 5.1. *Historical Validation*

Historical back-casting showed that the Bae model produced the highest 34-year mean buckling probability (0.080870), followed by the Sato (0.029694) and Meier (0.021988) models, likely because the Bae model accounts for train-induced dynamic effects. The historical back-casting results for each model are presented in Fig. 1.

Validation was performed using Bayes' theorem, with the prior probability $P(\text{Buckle})$estimated as 75/12417 from recorded events during 1990–2023. The distributions of $P(T_{rail} \mid \text{Buckle})$ and $P(T_{rail})$ were fitted by maximum likelihood estimation and selected using the K–S test, AIC, and BIC. Based on 10,000 simulations with truncated resampling excluding rail temperatures below 21.37 °C, the Bayesian estimate of $P(\text{Buckle} \mid T_{rail})$ was 0.00668097.

Because the Bayesian estimate represents the probability of at least one daily network-wide buckling event, whereas the physical models estimate failure probability for an individual 20 m track segment, the Monte Carlo results were converted to the network scale using a Poisson approximation and an effective number of representative segments. After conversion, the Bae model showed the smallest error 5.74% relative to the Bayesian estimate 0.0809, indicating the best agreement among the three models. The remaining discrepancy likely reflects underreporting in the historical event archive, suggesting that all models slightly underestimate actual buckling risk.

Under IPCC AR6, SSP1-2.6 to SSP5-8.5 represent progressively higher emissions pathways. Here, buckling probability denotes the arithmetic mean of model-estimated conditional probabilities across all analysis units within a given period and region, representing network-average rather than site-specific or joint-event risk.

### 5.2. *Prediction of Buckling Probability under Climate Scenarios*

To assess seasonal heat risk, June–September mean buckling probability was used as the reference metric. All three models showed little change under SSP1-2.6 but increasing trends under higher-emissions scenarios. The Bae model had the highest absolute risk and the strongest scenario divergence after around 2050, whereas the Sato model showed the largest relative increase despite lower absolute values; the Meier model remained the lowest ranking in relative increase. Detailed summer mean buckling probabilities for each model and scenario are presented in Fig. 2, Fig. 3, and Fig. 4.

The risk maps reveal clear spatiotemporal shifts across years and emissions pathways, with comparable buckling risk appearing earlier under higher-emissions scenarios. This pattern is illustrated in Fig. 5.–8., which present two maps for the Meier model, and two maps for the Bae model. For example, in the Bae model, the SSP5-8.5 risk pattern in 2080 is not reached under SSP3-7.0 until 2100, whereas in the Meier model, the SSP1-2.6 pattern in 2100 already emerges under SSP3-7.0 by 2050. These results indicate a clear temporal advancement of buckling risk under more intensive emissions pathways.

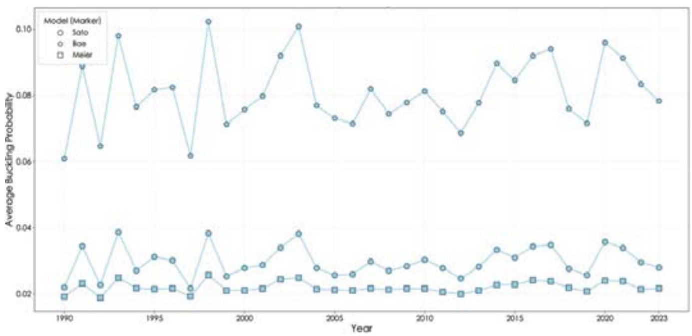


Fig. 1. Comparison of annual mean historical back-cast buckling probability across the three models

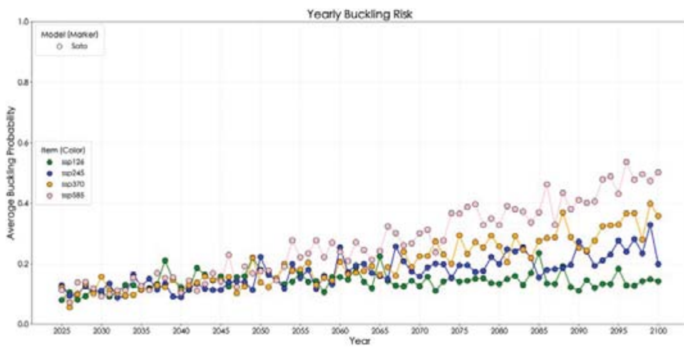


Fig. 2. Future mean buckling probability during summer months under different scenarios: Sato

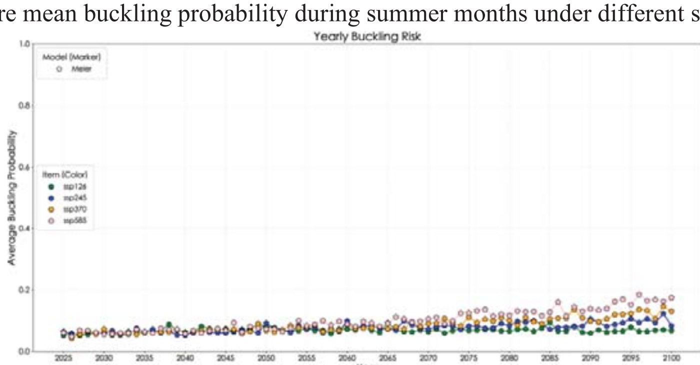


Fig. 3. Future mean buckling probability during summer months under different scenarios: Meier

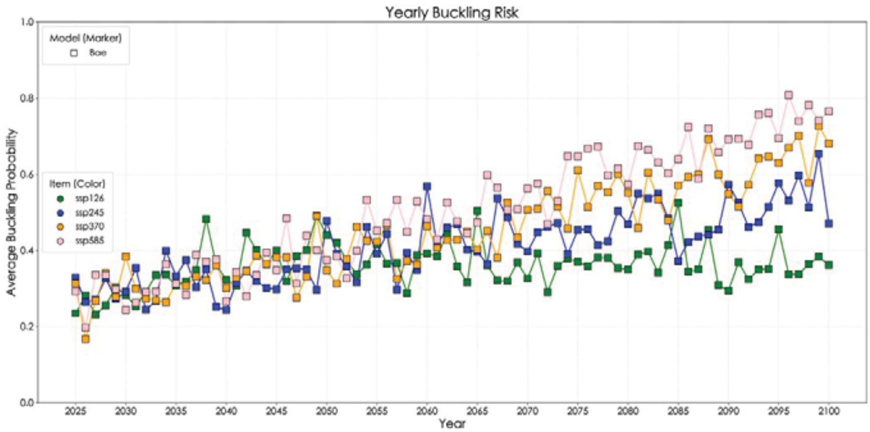


Fig. 4. Future mean buckling probability during summer months under different scenarios: Bae

Fig. 5. Buckling risk map of Taiwan in summer 2100 under SSP3-7.0 based on the Bae model.

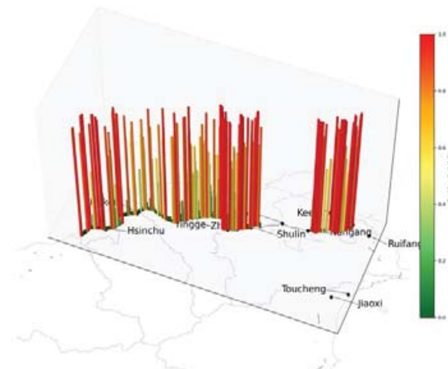


Fig. 7. Projected three-dimensional buckling risk surface of Meier model under SSP1-2.6 in 2100.

Fig. 6. Buckling risk map of Taiwan in summer 2080 under SSP5-8.5 based on the Bae model.

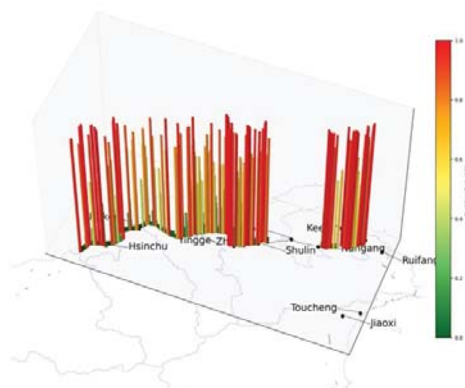


Fig. 8. Projected three-dimensional buckling risk surface of Meier model under SSP3-7.0 in 2050.

### 5.3. *Parameter Sensitivity and Monte Carlo Convergence Analysis*

The three-dimensional risk surfaces show clear spatial variability in buckling risk, driven mainly by curve radius and lateral ballast resistance. The Meier and Bae models are highly sensitive to sharp curvature, with risk rising rapidly below 500 m and exceeding 0.6 below 250 m, whereas the Sato model is much less curvature-sensitive. All three models also show substantial risk escalation under low lateral ballast resistance, especially below 250 kg/m. The vulnerability curves for curve radius and lateral ballast resistance are presented in Fig. 9. and 10., respectively.

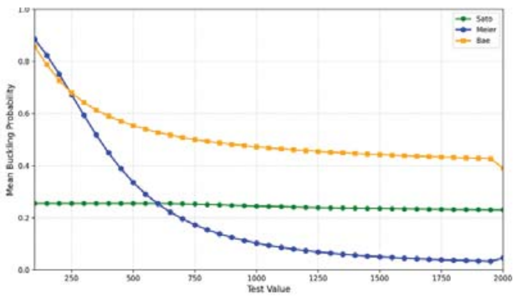


Fig. 9. Vulnerability curves of curve radius (m) for the three models.

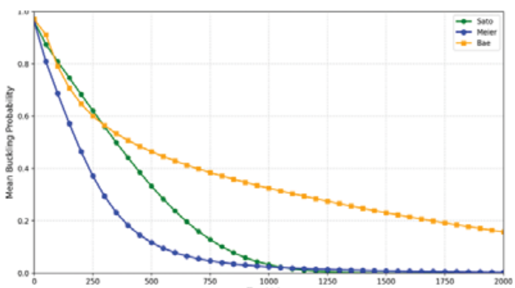


Fig. 10. Vulnerability curves of lateral ballast resistance (kg/m) for the three models.

To evaluate the adequacy of the Monte Carlo sample size, convergence analyses were conducted for all three models. Because the convergence behavior was similar, only the Bae model is shown in Fig. 11. as a representative example. Simulated values stabilized to within ±0.0001 (i.e., to the fourth decimal place) after approximately 1,000 iterations; therefore, 1,000 simulations were adopted to balance accuracy and computational efficiency. This suffices because the reported metric is an ensemble mean rather than a tail percentile; tail-focused analyses would require larger N.

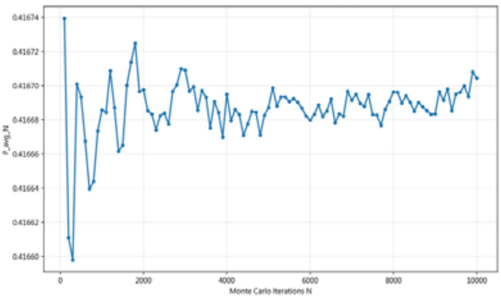


Fig. 11. Monte Carlo convergence of the Bae model

## 6. Conclusions and Recommendations

This study integrated three analytical buckling models (Meier, Sato, and Bae) with Monte Carlo simulation and IPCC AR6 climate projections to quantify heat-induced rail buckling risk on the TRC mainline. All three models consistently indicate that future probabilities rise to several times the historical back-cast baseline, with higher-emissions pathways advancing the temporal onset of critical risk and thereby compressing the window available for adaptation. Among the three, the Bae model showed the closest agreement with Bayesian validation after network-scale conversion, likely because it accounts for train-induced dynamic effects. Sensitivity analysis identifies curve radius and lateral ballast resistance as dominant factors.

For practical application, the risk maps and vulnerability curves offer a physics-grounded basis for prioritising adaptation. A Monte Carlo–driven graded warning system can translate projections into operational measures, while strategic upgrades — 50-to-60 kg rail replacement, selective ballastless-track conversion, and enhanced ballast maintenance — are expected to yield the greatest returns on high-risk curved segments. Mapping these tiers to explicit probability thresholds requires networkspecific cost-benefit analysis and is identified, alongside incorporating solar radiation into the rail–air temperature regression, as priority future work.

**Appendix A.** The Sato Model and Parameter Definitions

| Source | Model | Equation | |
|---|---|---|---|
| Huang (2022) | Sato Yoshihiko | $\frac{R}{100} < \frac{112.2J^{0.406}N_j^{0.333}}{g^{0.535}}$, | $P = 3.63J^{0.383}g^{0.535}N_j^{0.267}$ (A.1) |
| | | $\frac{R}{100} \geq \frac{112.2J^{0.406}N_j^{0.333}}{g^{0.535}}$, | $P = 3.81J^{0.383}g^{0.535}N_j^{0.267} - \frac{20.2J^{0.789}N_j^{0.6}}{R}$ (A.2) |
| | | **Parameter** | **Parameter Description** |
| | | $R$ | radius of curvature (cm) |
| | | $g$ | lateral ballast resistance (kg/cm) |
| | | $N_j$ | Track panel rigidity ratio (dimensionless) |
| | | $J$ | moment of inertia of rail about the vertical axis ($cm^4$) |

## References


Bae, Hyun-Ung, Jin-Yu Choi, Jiho Moon, and Nam-Hyoung Lim. "Development of a Probabilistic Buckling Analysis Scheme for Continuous Welded Rail Track." *Proceedings of the Institution of Mechanical Engineers, Part F: Journal of Rail and Rapid Transit* 229, no. 6 (2014): 1–12.

Chen, Yen-Hsi. "Lateral Resistance Measurement and Influencing Factors of Ballast." Master's thesis, National Cheng Kung University, 2019.

Chiang, Tzu-Fan**.** Effects of Ballast Resistance on Track Buckling Temperature. Master's thesis, National Cheng Kung University, 2017. [In Chinese]

Chinowsky, Paul, J. Helman, S. Gulati, J. Neumann, and J. Martinich. "Impacts of Climate Change on Operation of the US Rail Network." *Transport Policy* 75 (2019): 183–91.

Chu, Yu-Hsien. "Study on Rail Buckling Analysis and Fatigue Effect." Master's thesis, National Chung Hsing University, 2002. [In Chinese]

Dobney, K., C. J. Baker, L. Chapman, and A. D. Quinn. "Quantifying the Effects of High Summer Temperatures Due to Climate Change on Buckling and Rail Related Delays in South-East United Kingdom." *Meteorological Applications* 16 (2009): 245–51.

Han, Tsung-Hao. "Wireless Monitoring and Prediction Model of Rail Temperature." Master's thesis, National Cheng Kung University, 2015. [In Chinese]

Hu, Yi-Chin, Yen-Hung Chou, En-Te Lin, Chiung-Wen Chang, Pei-Yun Chu, Yi-Fei Chen, Wei-Yuan Hsiao, and Shih-Chin Lee. *Climate Change Risk Assessment on Transport Infrastructure and Advanced Risk Information Service Project: Final Report*. Taipei: Institute of Transportation, Ministry of Transportation and Communications, 2018. [In Chinese]

Huang, Min-Jen, and Chin-Liang Chang. *New Century Railway Engineering: Fundamentals*. 5th rev. ed. Taipei: Wensheng Book Co., 2022. [In Chinese]

Huang, Tsung-Hsin. *Comparative Study on Performance and Cost of Replacing 50KG and 60KG Rails by TRA*. Technical report. Chiayi: Chiayi Engineering Section, Taiwan Railway Administration, 2009. [In Chinese]

Kish, A., and G. Samavedam. "Dynamic Buckling of Continuous Welded Rail Track: Theory, Tests, and Safety Concepts." *Transportation Research Record* 1289 (1991): 23–38.

Luo, Kun-Long, Chao-Lieh Wang, Cheng-Hsin Chang, and Hsu-Ling Lin. "Study on Stress of Continuous Welded Rail of Yuanlin Elevated Railway." Paper no. 389 presented at the 10th National Conference on Structural Engineering, Taoyuan, Taiwan, December 1–3, 2010. [In Chinese]

Nguyen, Minh N., Xiaoming Wang, and Chi-Hsiang Wang. "A Reliability Assessment of Railway Track Buckling during an Extreme Heatwave." *Proceedings of the Institution of Mechanical Engineers, Part F: Journal of Rail and Rapid Transit* 226, no. 5 (2012): 513–17.

Taiwan Climate Change Projection Information and Adaptation Knowledge Platform (TCCIP). "Taiwan Climate Change Projection Information and Adaptation Knowledge Platform." Accessed August 29, 2025. https://tccip.ncdr.nat.gov.tw/.

Villalba Sanchis, I., R. Insa Franco, P. Martínez Fernández, P. Salvador Zuriaga, and J. B. Font Torres. "Risk of Increasing Temperature Due to Climate Change on High-Speed Rail Network in Spain." *Transportation Research Part D: Transport and Environment* 82 (2020): 102312.

Villalba Sanchis, I., R. Insa Franco, P. Salvador Zuriaga, and P. Martínez Fernández. "Risk of Increasing Temperature Due to Climate Change on Operation of the Spanish Rail Network." *Transportation Research Procedia* 45 (2020): 5–12.